

Computing Distance Distributions from Dipolar Evolution Data with Overtones: RIDME Spectroscopy with Gd(III)-Based Spin Labels

Katharina Keller,[†] Valerie Mertens,[†] Mian Qi,[‡] Anna I. Nalepa,[§] Adelheid Godt,[‡] Anton Savitsky,[§] Gunnar Jeschke,[†] and Maxim Yulikov^{*,†}

[†]Laboratory of Physical Chemistry, Department of Chemistry and Applied Biosciences, ETH Zurich, Vladimir-Prelog-Weg 2, 8093 Zurich, Switzerland

[‡]Faculty of Chemistry and Center for Molecular Materials (CM₂), Bielefeld University, Universitätsstraße 25, 33615 Bielefeld, Germany

[§]Max Planck Institute for Chemical Energy Conversion, Stiftstrasse 34-36, D-45470 Mülheim an der Ruhr, Germany

Supplementary Information

OvertoneAnalysis

The software package *OvertoneAnalysis* is based on the open-source DeerAnalysis package.¹ It is executed via MATLAB. The package differs from DeerAnalysis by using an extended kernel function in the Tikhonov regularization procedure to account for frequency overtones according to

$$K_{mod}(r) = \int [P_1 \cdot \cos(\omega(r, \theta) \cdot t) + P_2 \cdot \cos(2\omega(r, \theta) \cdot t) + P_3 \cdot \cos(3\omega(r, \theta) \cdot t)] \cdot \sin(\theta) d\theta.$$

The fraction of the first (P_2) and second harmonic (P_3) overtone can be adjusted in the graphical user interface of *OvertoneAnalysis* (see Figure S1), while the fraction of the fundamental frequency (P_1) is given by the requirement that the total sum of all three coefficients is one ($P_1 = 1 - P_2 - P_3$). Yet higher harmonic overtones are neglected since their contributions to the RIDME signals was unmeasurably small in the experimental data acquired to date.

Tikhonov regularization is then performed using the modified kernel function with the given fractions P_i . The extraction of the obtained distance information can be performed in analogy to the procedure described for the DeerAnalysis software package.

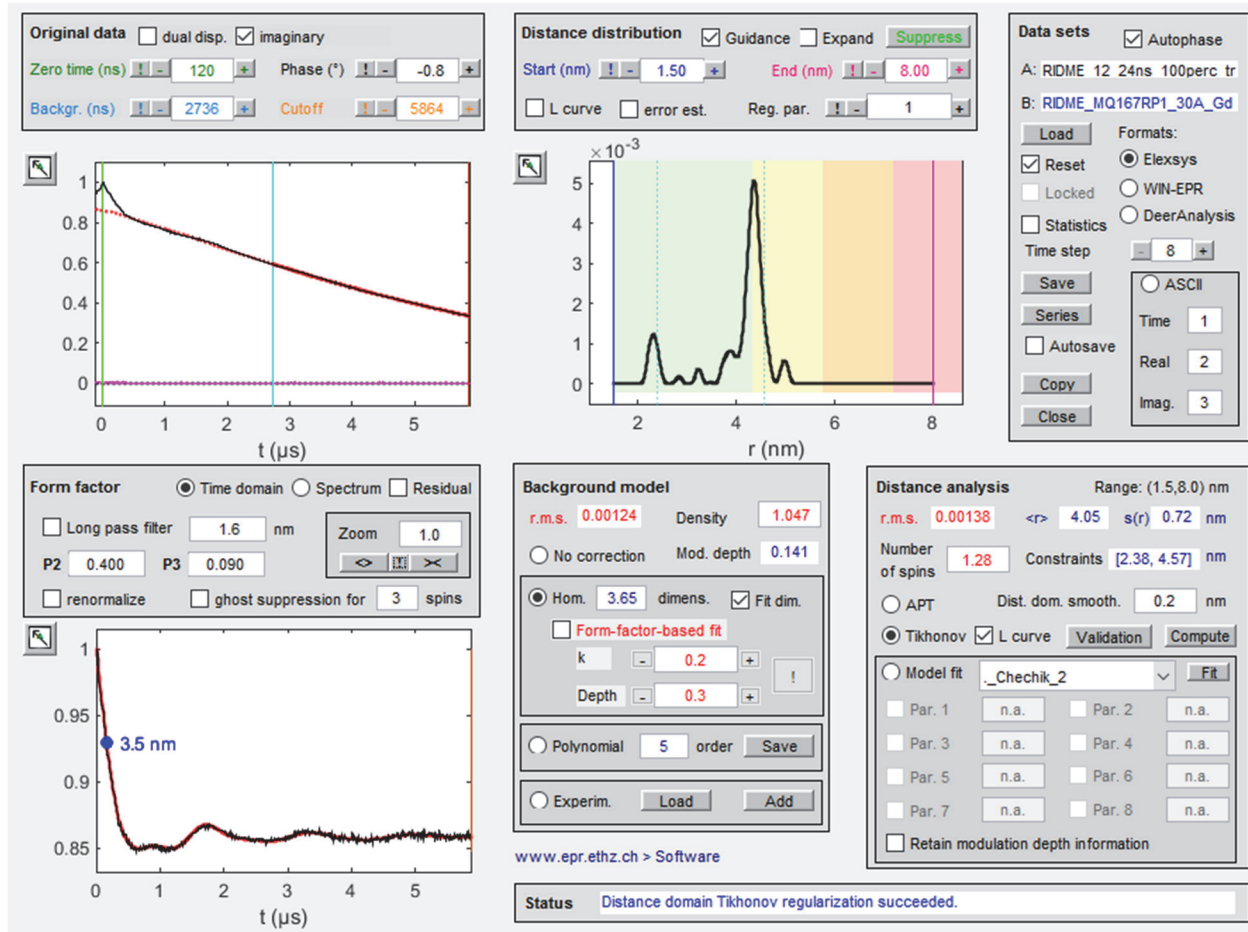


Figure S1: Graphical interface of *OvertoneAnalysis*.

In analogy to DeerAnalysis, the software package provides tools required for pre-processing of RIDME raw data as well as for the subsequent computation of the underlying distance distributions. After loading the experimental data in the designated Data sets panel, the primary RIDME data are displayed in the Original data section of the graphical interface of *OvertoneAnalysis* (see Figure S1, top left corner). Pre-processing of the time traces should be performed by adjusting zero time and the phase of the signal.

However, the background decay and thus its correction differ between DEER and RIDME. For RIDME data it is important to fit the correct background dimensionality of the homogenous distribution, as it is dependent on the experimental conditions. In most of the cases at hand, due to the observable oscillations in the form factor traces, the background correction by stretched exponential model functions can be considered to be accurate. It was found that the optimum range for the background fit is located towards the end of the signal, where the contribution of dipolar oscillations has already almost decayed. The part of the signal which is utilized for fitting the background function is specified by the Backgr. edit field, which determines the starting point, and the Cutoff edit field, which marks the end of the considered part of the signal and thus the end of the range used for background fitting. The chosen interval is visualized by a blue and an orange line within the graphic (see Figure S1, top left corner). In general, it is desirable to consider as much of the measured signal as possible. However, due to the fact that the RIDME background decay

can be quite steep and that background correction involves division of the initial time trace by the background function, it is possible that the form factor (bottom left corner) is noisy towards the end of the trace (see Figure S2). In such cases, or when artefacts at the end of the time domain data are present, cut-off at earlier times is required. Cutting off a significant amount of data will suppress noise, but background correction may become more difficult and will cause the suppression of long distances. In the studied data set, the range for background fitting, which was found automatically by pressing the two relevant ‘!’ buttons resulted in a reasonable background model. Nevertheless, it was verified for every investigated data set that the form factor in time and frequency domain exhibited the expected shape after removing the background contribution. For the form factor in time domain, this means a decay to a constant value and thus a flat line towards the end of the RIDME trace if the oscillations are completely decayed.

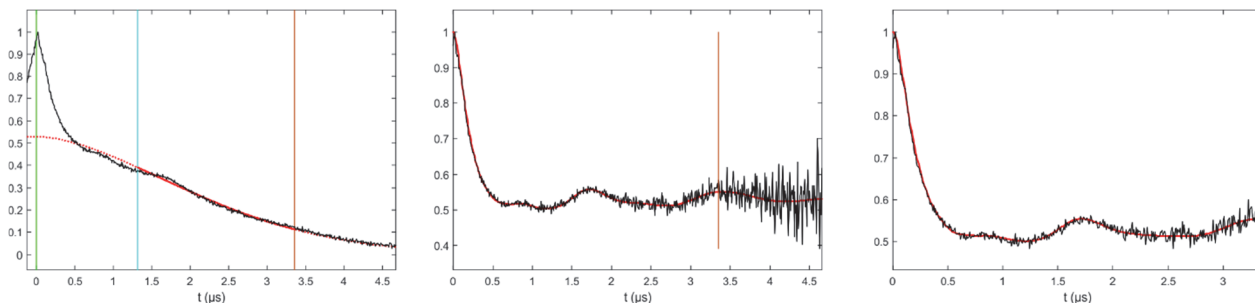


Figure S2: Noise truncation by trace cut-off for the Gd-ruler 2_2 . Measured at 20 K using a mixing time of 24 μs .

Tikhonov regularization can then be executed using the modified kernel functions as well as different regularization parameters α . From the resulting L curve (Distance distribution panel), α_{opt} was determined (see DeerAnalysis manual, Figure S3) and the corresponding distance distributions is displayed. As for DEER experiments, the reliability of distance distributions depends strongly on the maximum dipolar evolution time. Thus, the color coding for reliability ranges in the Distance distribution panel are analogous to DeerAnalysis. Pale green: Shape of distance distribution is reliable. Pale yellow: Mean distance and width are reliable. Pale orange: Mean distance is reliable. Pale red: Long-range distance contributions may be detectable, but cannot be quantified. A scheme of the different steps within the analysis program is given in Figure S3. For more details on the analysis program refer to the DeerAnalysis manual.

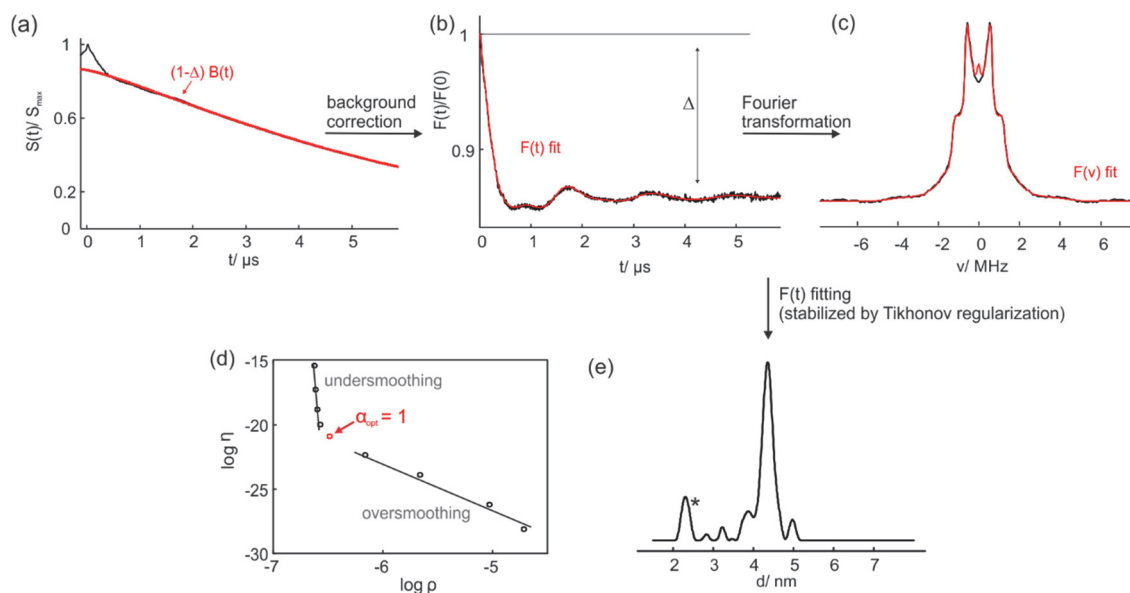


Figure S3: Schematic representation for the extraction of distance distributions from RIDME raw data presented for the Gd-ruler **2₂** (10 K, 8 μ s). a) normalized and phase-corrected primary RIDME data (black line) with background fit (red line); b) RIDME form factor in time domain obtained after background correction and subsequent renormalization (black line) and its fit (red line); c) RIDME form factor in frequency domain (black line) and its fit (red line); d) L-curve resulting from Tikhonov regularization using the extended kernel function and different regularization parameters; e) resulting distance distribution $p(r)$ obtained by Tikhonov regularization with the extended kernel function (*artefact resulting from echo crossing).

Note that in the newest version of the DeerAnalysis software the fast Tikhonov regularization routines from Prof. P.C. Hansen (DTU) are used, which do not include the non-negativity constraint. The final calculation of the distance distribution with the selected regularization parameter is then done by considering the non-negativity condition. The published version of the *OvertoneAnalysis* software, being a ‘daughter’ of DeerAnalysis, is also based on this fast version of the Tikhonov regularization. However, the data analysis presented in this paper was still performed using the previous, slower version of the Tikhonov regularization procedure, including the non-negativity constraint at every step. Furthermore, both approaches use different definitions of the regularization parameter. For simulated data using a Gaussian distribution with FWHM of 0.5 nm and 3.4 nm mean distance, the value of 1, used in this work, corresponds to a value of 100 in the published version of *OvertoneAnalysis*. The old version of the software is available from the authors upon request.

A comparison of data analysis using an ‘overtone-free’ or an ‘overtone-containing’ kernel is shown in Figure S4a for simulated data (3.4 nm mean distance, Gaussian distribution with a FWHM of 0.5 nm, $\{P_{1,\text{sim}} = 0.4, P_{2,\text{sim}} = 0.5$ and $P_{3,\text{sim}} = 0.1\}$) and in Figure S4b for an experimental dataset (Gd-ruler **2₂**).

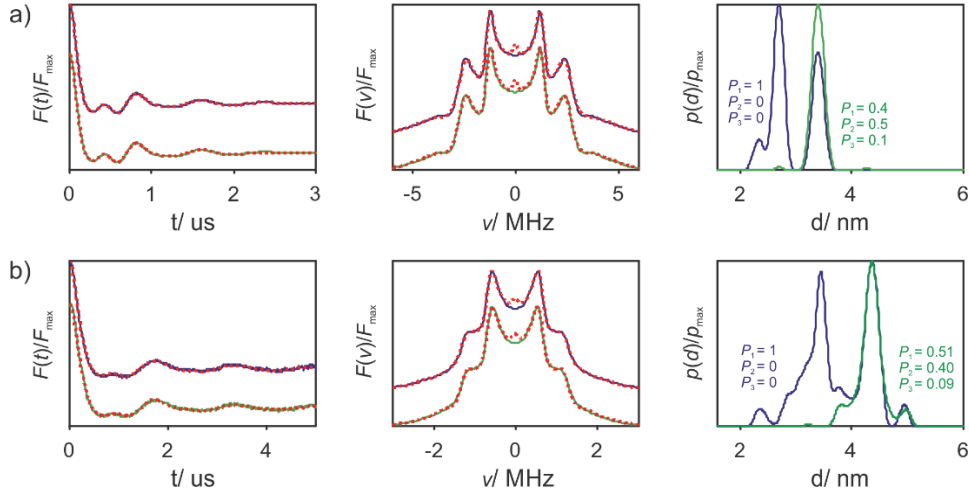


Figure S4: Comparison of data analysis using an ‘overtone-free’ (purple line) and an ‘overtone-containing’ kernel (green line). a) Simulated data of a Gaussian distribution with 3.4 nm mean distance, FWHM of 0.5 nm, modulation depth of 30 % and coefficients $P_{1,\text{sim}} = 0.4$, $P_{2,\text{sim}} = 0.5$ and $P_{3,\text{sim}} = 0.1$). The coefficients were set to the simulated values $\{P_1 = 0.4; P_2 = 0.5; P_3 = 0.1\}$ in the ‘overtone-containing’ kernel. b) Gd-ruler 2_2 measured at W-Band, 10 K and 8 μs mixing time. The raw data were truncated as described below resulting into a modulation depth of 12%. The coefficients were set to $\{P_1 = 0.51; P_2 = 0.40; P_3 = 0.09\}$ in the ‘overtone-containing’ kernel. From left to right: form factors and corresponding fits (red dashed lines), dipolar spectra and corresponding fits (red dashed lines), computed distance distribution and simulated distance distribution (black dashed lines).

Experimental set-up and measurement conditions

The RIDME pulse sequence creates a multitude of echoes. Thus, precise phase cycling is required to remove echo crossings and it is important to carefully adjust the phase settings prior to performing the RIDME experiment. Importantly, the amplification of the signal has to be adjusted at zero time of the dipolar evolution ($d_{12} = 0$) when the stimulated echo and the primary echo from the last two pulses fall on top of the refocused virtual echo, which is used for detection (see Figure S5b). This situation corresponds to the largest total echo amplitude encountered during the whole experiment. The strong appearance of the stimulated echo as well as the primary echo from the last two pulses in the sequence can also be used to find the detected RIDME echo during set up: at $d_{12} = d_{12,\text{init}} = -120$ ns three echoes (Figure S5a) can be observed, while at $d_{12} = 0$ the stimulated and primary echo will fall on top of the RIDME echo as shown in Figure S5b.

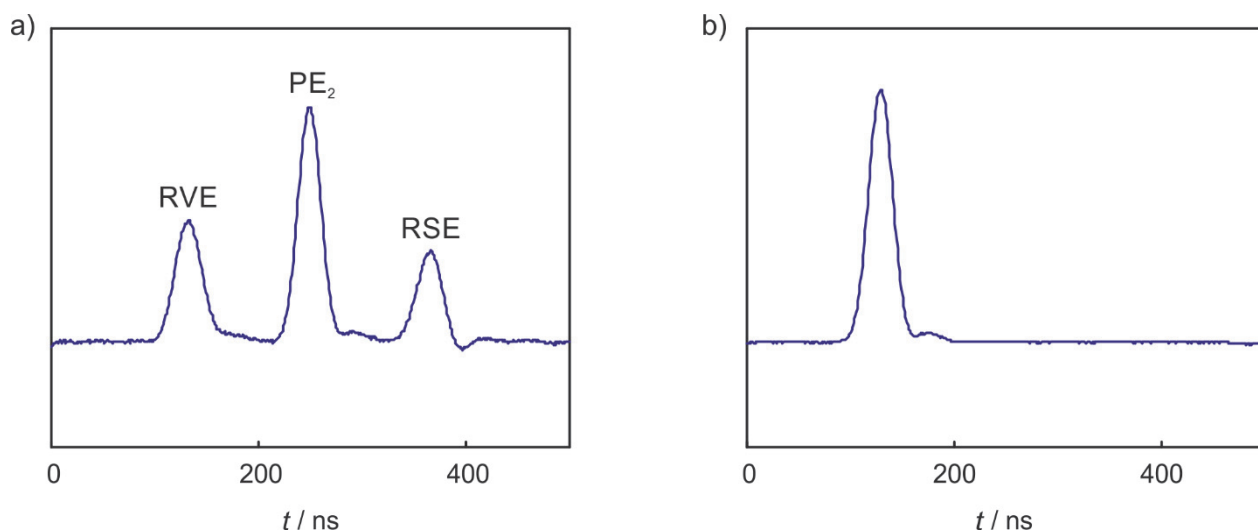


Figure S5: Echoes resulting from the RIDME pulse sequence at the detection position. The refocused virtual echo (RVE, used for detection) occurs at $t_{RVE} = 2d_1 + 2d_2 + d_4$, while the stimulated echo (RSE) occurs at $t_{RSE} = t_{RVE} - 2d_{12}$ and the primary echo from the last two pulses (PE_2) at $t_{PE_2} = t_{RVE} - d_{12}$. Thus, the PE_2 and RSE change their position during the experiment, and cause echo crossings. Two different situations are displayed for a) $d_{12} = -120$ ns and b) $d_{12} = 0$.

The strongest artefacts that can be observed during measurements are caused by the three echoes shown above. Note that further artefacts were sometimes observed at $t = 2d_1$ and at $t = d_2 - d_1$, which may distort the primary data and thus the distance distributions. The artefact level is dependent on the mixing time T_{mix} . For short mixing times $T_{mix} < T_m$ a higher artefact level was observed, resulting from an incomplete decay of the components of the transverse magnetization during the mixing block. Contrary, a very long mixing block increases the relative contribution of the primary echo (PE_2) from the last $\pi/2$ and π pulse, thus increasing the spike-like artefact around zero time.

On another note, temperature (changes in relaxation properties) and mixing time influence modulation depth (m.d.) as well as background decay. For higher temperatures and longer mixing times the background decay is steeper, thus limiting the maximum detectable distance and reducing SNR. On the other hand, the m.d. is increased at those conditions. The maximum m.d. in the high temperature limit is expected to achieve $\lambda = 1 - 1/(2S+1)$ giving a value of 0.875 for Gd(III) in comparison for 0.5 for spin $S = 1/2$ systems.² Figure S6 shows some of the properties related to temperature and mixing time for the Gd(III) ruler **13**.

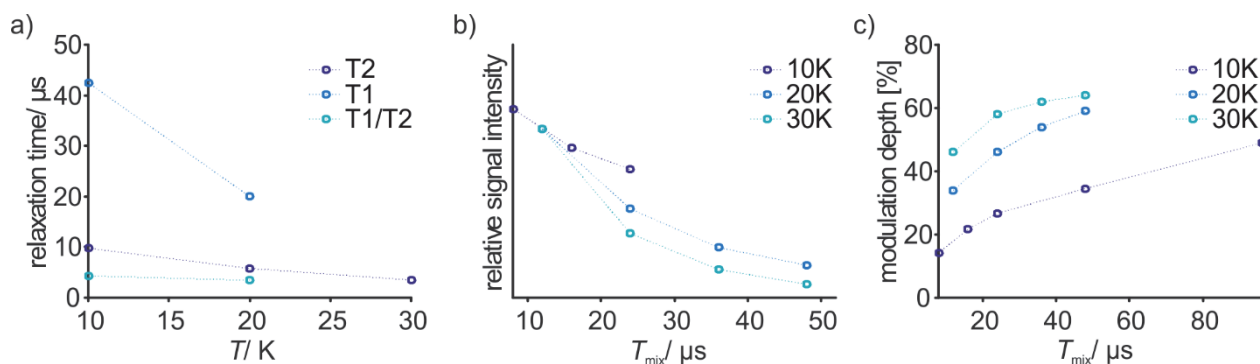


Figure S6: Dependence of a) relaxation times, b) relative signal intensity (scaled to the signal intensity corresponding to 12 μs mixing time) and c) modulation depth on mixing time and temperature for the Gd-ruler 13.

Extraction of overtone coefficients for broad distance distributions

Figure S7-S9 show the decrease of overtone specific features upon broadening of the distance distribution. Thus, the higher-frequency overtones can no longer be identified in time- and frequency-domain data. Besides, the distance distribution does not exhibit artefacts peaks, but starts to become asymmetric. The mean distance is shifted for broad distributions if the overtone coefficients are mismatched. In such cases, either an *a priori* knowledge of the overtone coefficients is needed, or, for calibration, a control measurement using the DEER technique should be available. The latter strategy may run into problems for short distances, due to the distortion of distance distributions in the DEER experiments with high-spin centers. In that case, a CIDME³ control measurement may be preferable.

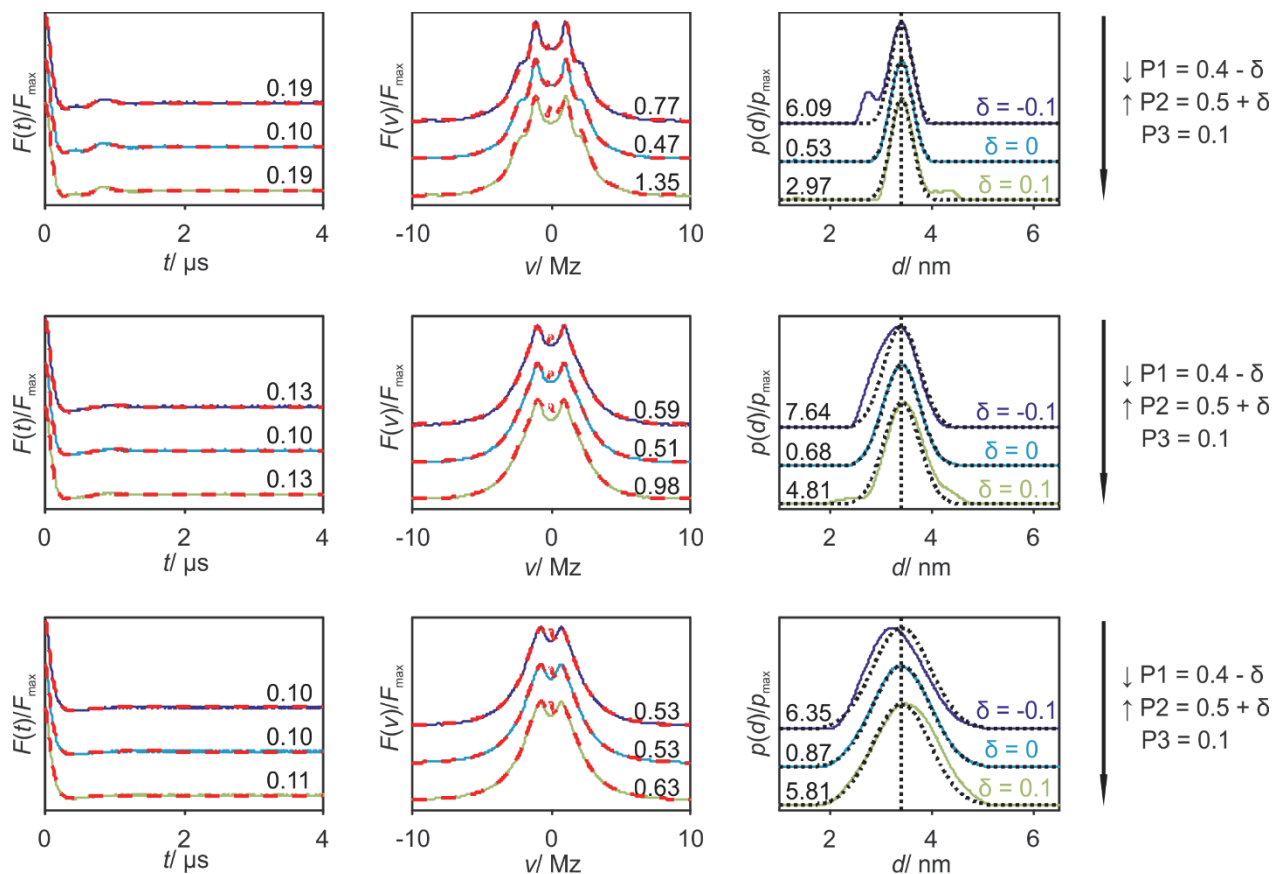


Figure S7: Influence of the distance distribution width on dipolar evolution data with harmonic overtones studied on simulated data: Gaussian distribution with increasing width from top to bottom, 3.4 nm mean distance (indicated by black dashed vertical lines), added white noise, 30% modulation depth. The coefficients were set to $P_{1,\text{sim}} = 0.4$, $P_{2,\text{sim}} = 0.5$ and $P_{3,\text{sim}} = 0.1$. Variation of coefficients P_1 and P_2 , P_3 is kept constant. δ gives the deviation of P_1 from the simulated fraction $P_{1,\text{sim}}$. RMSD values (multiplied by a factor of 100) between the data trace and the different fits or

the computed and the simulated distance distribution are displayed at the corresponding trace. From left to right: form factors and corresponding fits (red dashed lines), dipolar spectra and corresponding fits (red dashed lines), computed distance distribution and simulated distance distribution (black dashed lines).

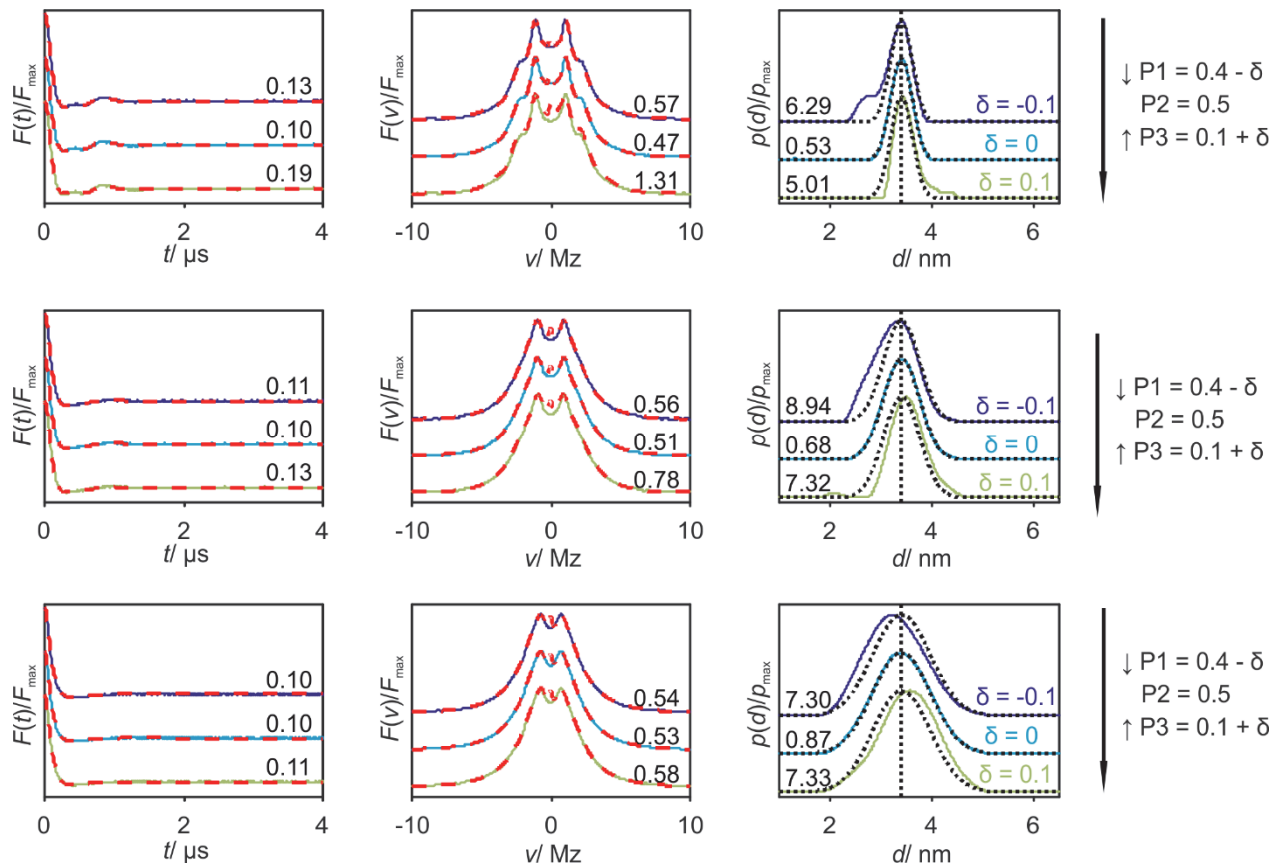


Figure S8: Influence of the distance distribution width on dipolar evolution data with harmonic overtones studied on simulated data: Gaussian distribution with increasing width from top to bottom, 3.4 nm mean distance (indicated by black dashed vertical lines), added white noise, 30% modulation depth. The coefficients were set to $P_{1,\text{sim}} = 0.4$, $P_{2,\text{sim}} = 0.5$ and $P_{3,\text{sim}} = 0.1$. Variation of coefficients P_1 and P_3 , P_2 is kept constant. δ gives the deviation of P_1 from the simulated fraction $P_{1,\text{sim}}$. RMSD values (multiplied by a factor of 100) between the data trace and the different fits or the computed and the simulated distance distribution are displayed at the corresponding trace. From left to right: form factors and corresponding fits (red dashed lines), dipolar spectra and corresponding fits (red dashed lines), computed distance distribution and simulated distance distribution (black dashed lines).

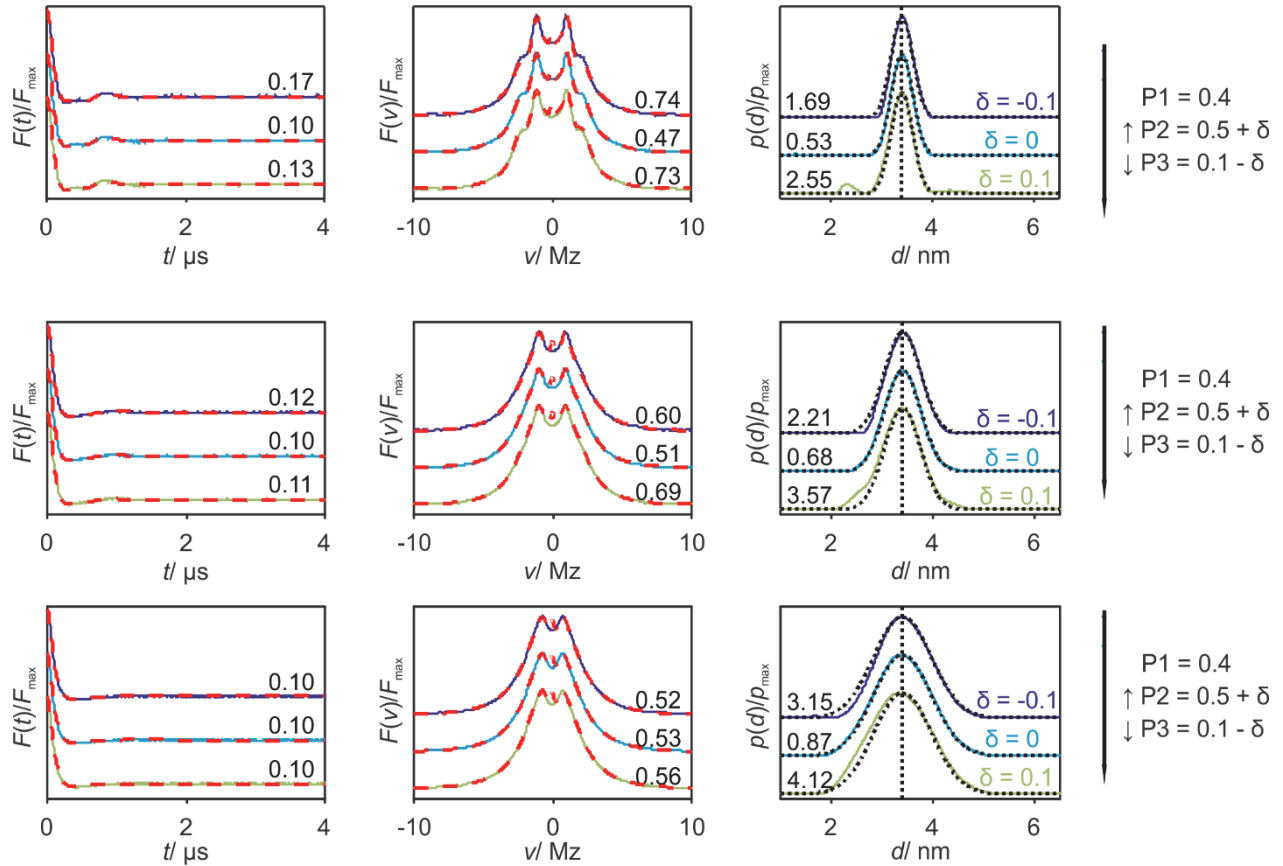


Figure S9: Influence of the distance distribution width on dipolar evolution data with harmonic overtones studied on simulated data: Gaussian distribution with increasing width from top to bottom, 3.4 nm mean distance (indicated by black dashed vertical lines) added white noise, 30% modulation depth. The coefficients were set to $P_{1,\text{sim}} = 0.4$, $P_{2,\text{sim}} = 0.5$ and $P_{3,\text{sim}} = 0.1$. Variation of coefficients P_2 and P_3 , P_1 is kept constant. δ gives the deviation of P_i from the simulated fraction $P_{i,\text{sim}}$. RMSD values (multiplied by a factor of 100) between the data trace and the different fits or the computed and the simulated distance distribution are displayed at the corresponding trace. From left to right: form factors and corresponding fits (red dashed lines), dipolar spectra and corresponding fits (red dashed lines), computed distance distribution and simulated distance distribution (black dashed lines).

Filtering artefact due to echo-crossing for long distances

Figure S10 shows the dependence of the maximum signal intensity of the time trace on the pulse length. As described in the main text, the maximum is expected to be at the time where the three echoes cross ($d_{12} = 0$). However, experimentally we observe a shift of the apparent zero time from the expected value (d_0) by about the difference between the length of the π and the $\pi/2$ pulse. As the echoes cross at $d_0 + t_p(\pi) - t_p(\pi/2)$, the shift in zero time can be avoided by making pulses all of the same length.

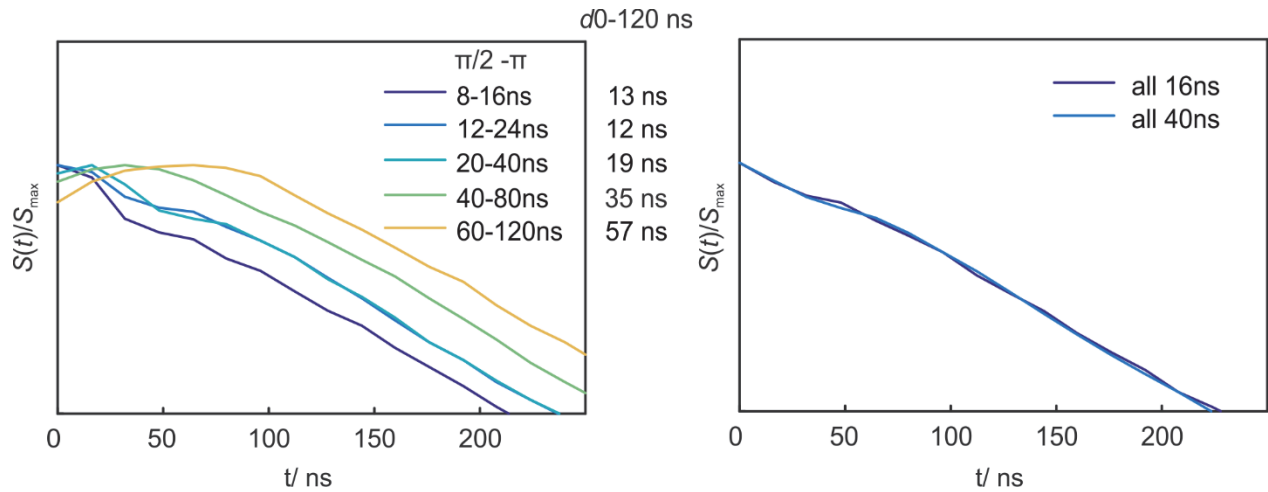


Figure S10: Influence of the pulse length on the position of the maximum of RIDME signal measured for the Gd-ruler **15** at 20 K and 20 μ s mixing time. Left: $\pi/2 - \pi$ pulses with $t(\pi) = 2 * t(\pi/2)$. Right: $\pi/2 - \pi$ pulses of equal length.

If phase cycling is incomplete, the echo crossing introduces an artefact in the RIDME primary data. The artefact in the primary data in turn causes a short distance artefact in the distance distribution, which could not be related to overtone coefficients. If this bump-like artefact can be clearly identified (e.g. for long distances, where the true dipolar oscillation is much slower) it can be filtered out from the primary data (see Figure S11 for the samples studied here). It is seen, that truncation of the bump artefact reduces m.d., but does not change the shape of the overall form factor and artefacts peaks < 3 nm can be filtered out. Furthermore, it is observed that the choice of zero time does not change the distance distribution significantly. However, it might become important if small changes need to be detected.

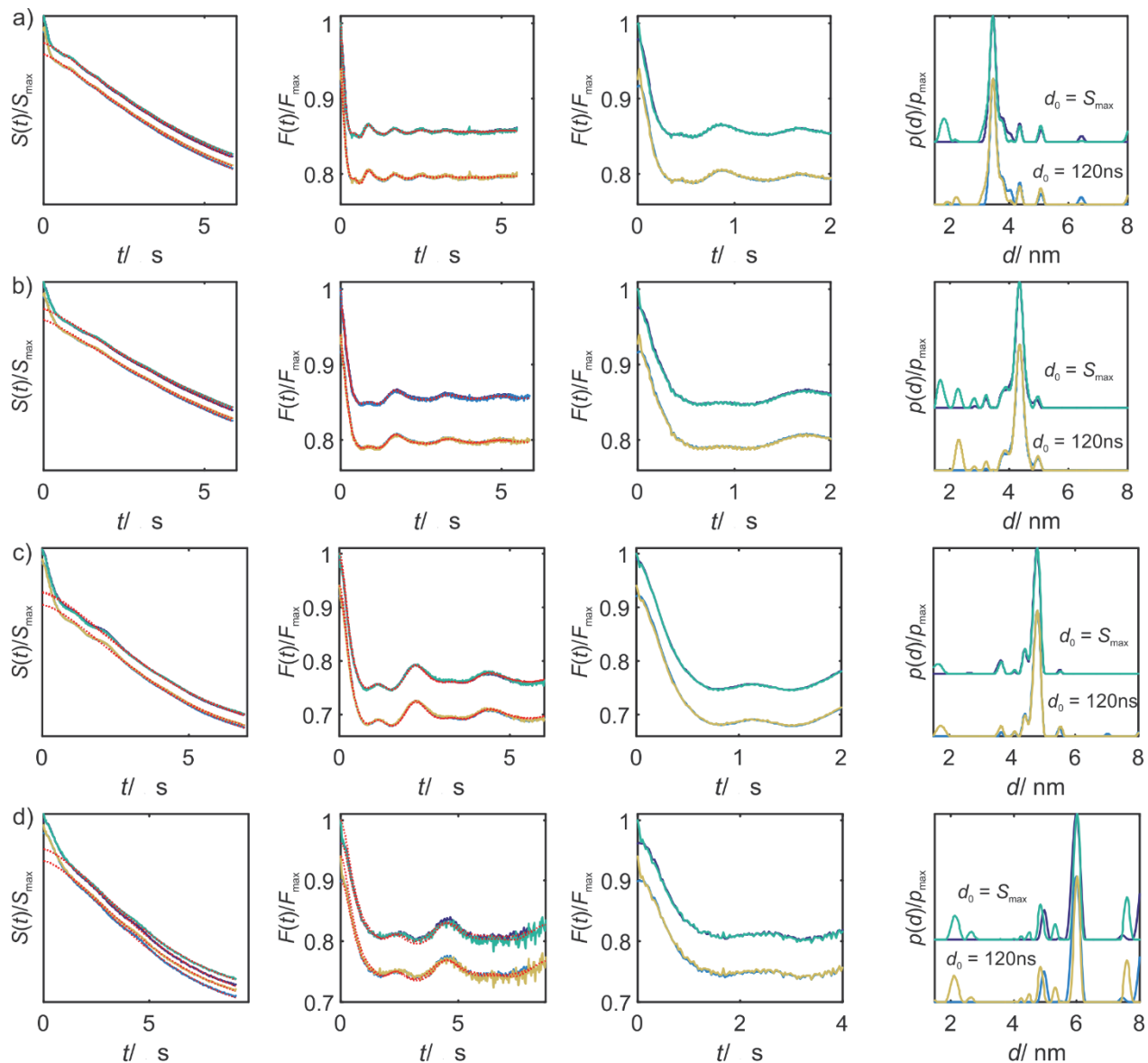


Figure S11: Examples for filtering the bump-like artefact at zero time and influence of the choice of zero time on the distance distribution. a) Gd-ruler **1₃** (10 K, 8 μ s), b) Gd-ruler **2₂** (10 K, 8 μ s), c) Gd-ruler **1₅** (10 K, 24 μ s) and d) Gd-ruler **1₇** (10 K, 16 μ s). For each subfigure: for the two upper lines zero time set to apparent maximum, RIDME raw data colored in violet and truncated data in turquoise and for the two lower lines zero time set to 120 ns, RIDME raw data colored in light blue and truncated data in yellow. Truncated data are y-shifted by the artefact amplitude.

The filtering approach is based on the fact that short distance artefacts in the distance distribution correspond to high-frequency components in the time domain signal. In principle, such high-frequency components can be removed from the time trace by applying a digital low-pass filter, which in turn suppresses the short-distance artefacts. However, since this procedure also removes high-frequency noise, the original and the filtered data differ more than only by the unwanted, artefact-inducing frequency components, which is often not desired. This problem can be circumvented by subtracting the filtered data from the original primary data and only removing those components of the residual from the original signal that exceed the noise level. Doing so, the resulting time-domain signal differs

from the original signal only by the absence of the unwanted high-frequency components. Such signals are referred to as truncated signals in this work. The described filtering procedure was performed for selected data sets of Gd-rulers **1**₃, **1**₅, **1**₇, and **2**₂. The resulting primary data and the change in distance distribution are shown in Figure S11. To discuss the effect of truncation we will look at the example shown in Figures S12. It is based on a Butterworth digital low pass filter and utilizes the MATLAB function *butter*. Its magnitude and phase response function is plotted in Figure S12a and can be modified by the cutoff frequency and filter order. The resulting filtered data y_{filt} (red line) are shown in Figure S12b on top of the RIDME raw data y (blue line). From filtered and raw primary data, truncated data y_{trunc} (green line) (Figure S12c) are created as described above and are plotted on top of the RIDME raw data (blue line, Figure S12c). The main deviation between the two time traces is observed in the region around the maxima. When adjusting the zero time, as demanded by theory, to 120 ns, this region coincides with the time origin of the primary signal. The high-frequency components, which are assumed to cause the observed short distance artefacts in the distance distribution (at $r < 3$ nm), therefore only contribute to the signal at initial times and manifest in terms of a bump-like artefact. This artefact in turn explains the observed non-coincidence of origin and maximum of the original primary signal as well as the observed sensitivity of the short distance artefacts in the distance distribution towards shifts in the zero-time (Figures S11 and S13-15). It is assumed, that such distortion of the time trace at initial times is caused by echo crossings and may thus be attributed to incomplete phase-cycling.

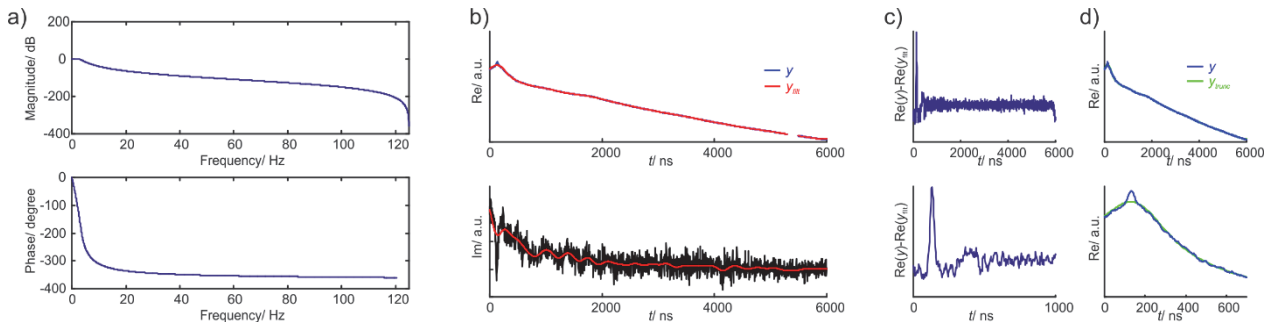


Figure S12: Example of filtering RIDME raw data for the Gd-ruler **2**₂ at 10 K and 8 μ s mixing time. a) Magnitude (top) and phase (bottom) response function of the filter, b) real (top) and imaginary (bottom) RIDME raw data y (blue line) and data resulting from filtering y_{filt} (red line), c) left residual between RIDME raw and d) filtered data and right truncated RIDME data y_{trunc} (green line) overlaid with the detected RIDME raw data (real part). c, d) The top line shows the complete trace, while the lower row shows an enlargement of the region around maximal signal intensity.

Extraction of distance distributions for short distances (Gd-ruler **1**₁)

Figure S13 shows the extraction of the distance distribution for the Gd-ruler **1**₁. If detection is performed at the maximum of the Gd(III) spectrum (Figure S13, top row), Tikhonov regularization with coefficients $P_2 = P_3 = 0$ (cyan and violet line) results in the lowest level of artefacts. Nevertheless, the uncertainty in zero time (theoretical value of 120 ns versus maximal signal intensity) does change the level of artefacts and thus the overtone coefficients dramatically. With increasing field offset, dipolar frequencies of the harmonic overtones become more pronounced. This leads to a change in artefact level for the same overtone coefficients at different detection positions. Choosing

the zero time at the maximum signal intensity of the primary traces yields, for the largest field offset, good agreement with the same set of coefficients as extracted for the other distances (bottom row, lower lines, yellow line). Setting the zero time to 120 ns indicates best agreement for a smaller contribution of P_2 and P_3 (bottom row, upper lines, blue line). This dependence of overtone coefficients on zero time is observed through all detection positions.

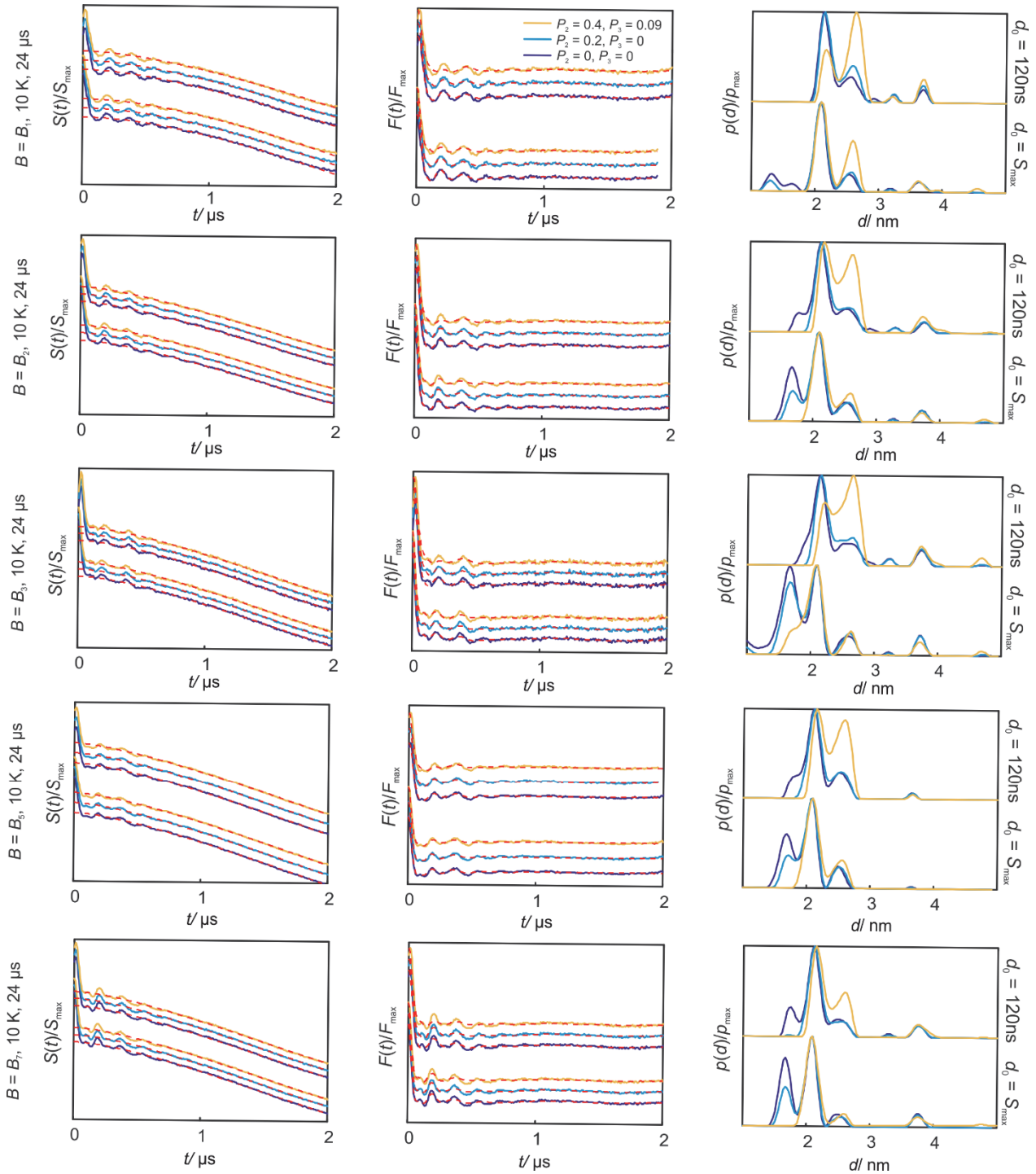


Figure S13: Extraction of overtone coefficients for the Gd-ruler 1_1 . RIDME data were acquired at different field

positions of the Gd(III) spectrum (see Figure 12 of the main text) at 10 K and a mixing time of 24 μs . From left to right: Primary RIDME data (solid line) and corresponding background fit (red dashes line), background corrected form factor (solid line) and its fit (red dashed line), resulting distance distribution. The color coding of the solid lines corresponds to a set of overtone coefficients and is retained throughout the whole figure. For each subfigure: zero time set to 120 ns for the upper lines and zero time set to apparent maximum for the lower lines.

To avoid the uncertainty in zero time, measurements were performed with $\pi/2$ and π pulses of equal length at three different detection positions (B_1, B_2, B_3 , see Figure 12). The results are displayed in Figure S14. Comparing the artefact level in the distance distribution it can be noted that the analysis with the zero time chosen at the maximum of the RIDME signal for 16-32 ns pulses and all 16 ns pulses yields very similar distance distributions. The small remaining differences may result from the different excitation bandwidth of the A spins. This effect is further studied in Figure S15. However, remaining uncertainties from imperfect phase cycling cannot be excluded. Based on these results we suggest to set the zero time close to the maximum signal intensity prior to Tikhonov regularization. For longer distances this uncertainty does not change the overtone coefficients or extraction of distances (see Figure S11), for short distances ($d < 3$ nm) this should be carefully investigated.

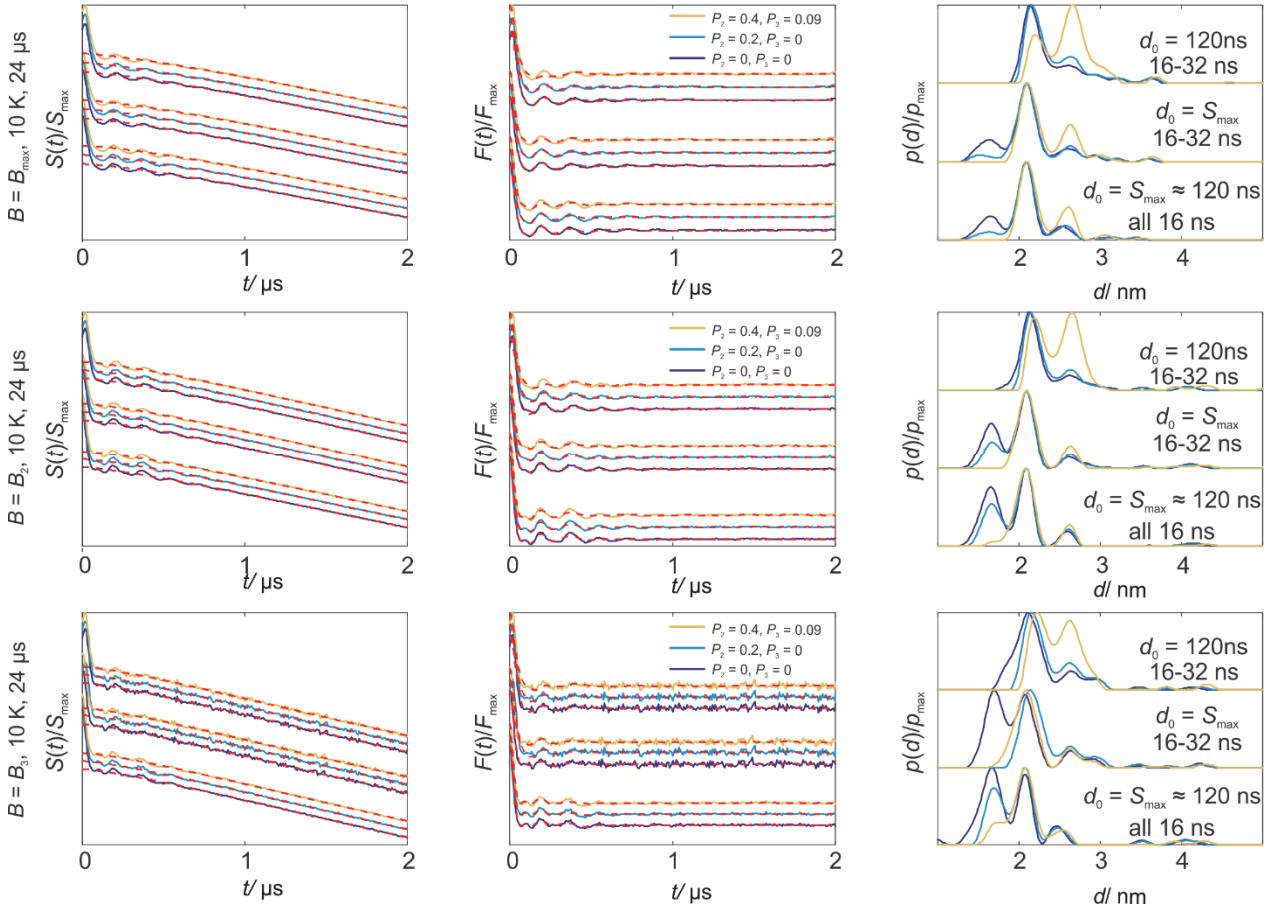


Figure S14: Extraction of overtone coefficients for the Gd-ruler $\mathbf{1}_1$ using different pulses settings. RIDME data were acquired at different field positions of the Gd(III) spectrum (see Figure 12 of the main text) at 10 K and a mixing

time of 24 μs . From left to right: Primary RIDME data (solid line) and corresponding background fit (red dashed line), background corrected form factor (solid line) and its fit (red dashed line), resulting distance distribution. The color coding of the solid lines corresponds to a set of overtone coefficients and is retained throughout the whole figure. The pulse length, for $(\pi/2)$ and (π) pulses, is given in the figure next to the corresponding distance distributions.

Figure S15 shows the effect of the observer pulse (A spin) bandwidth at two different detection positions for the Gd-ruler **11**. Long, selective pulses only burn a narrow hole in the Gd(III) spectrum and thus only excite a small fraction of spins within a narrow frequency range. In these cases, higher harmonics are even more suppressed and the shape of the primary data gets distorted. For the very soft 80 ns pulses, the corresponding excitation bandwidth of 12 MHz, is already smaller than the width of the Pake pattern of the primary dipolar harmonic at the given average distance of 2.1 nm. Higher dipolar overtones are then strongly suppressed, and due to the incomplete Pake pattern excitation, artefacts at longer distances appear in the distance distribution for the case $P_2 = P_3 = 0$. Small changes in the shape of distance distribution, computed with the ‘standard’ set of dipolar overtone coefficients $\{P_1 = 0.51, P_2 = 0.4, P_3 = 0.09\}$, are already observed for short pulses (16 or 32 ns), which also lead to small deviations of the “ideal” overtone coefficients. However, these effects are minor and differences of the coefficients are expected to be small, but may explain the remaining difference between $\pi/2$, π pulses of equal length with respect to π pulses being twice as long as $\pi/2$ pulses.

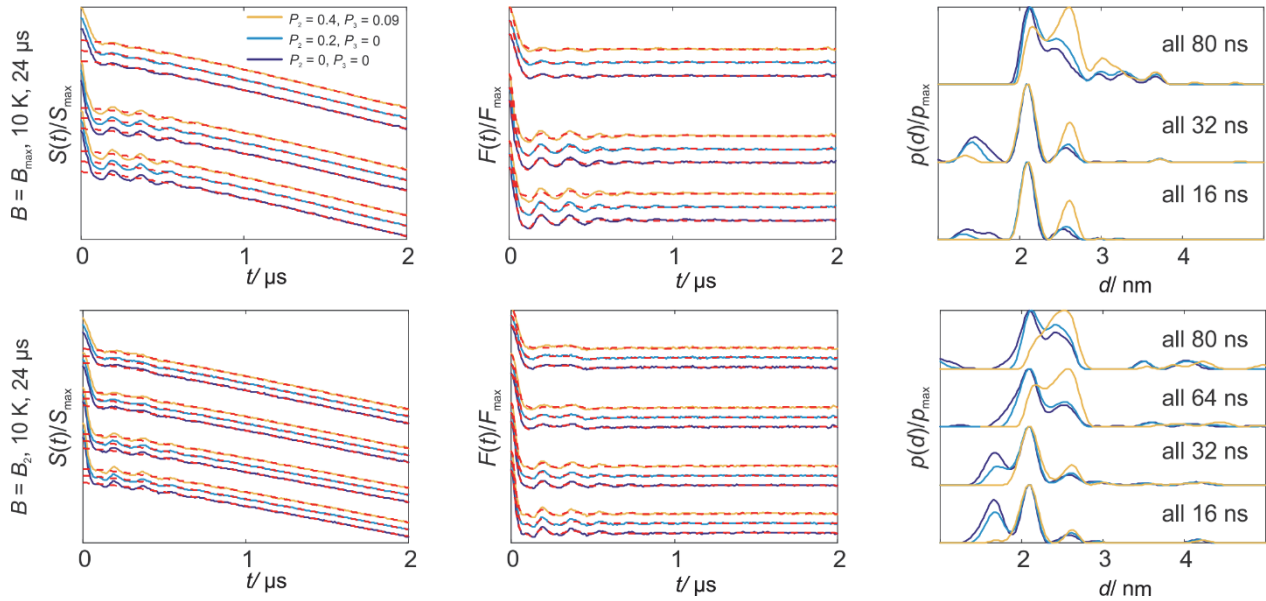


Figure S15: Extraction of overtone coefficients for the Gd-ruler **11** using $(\pi/2)$ - (π) pulses of the same length, with varying bandwidth. RIDME data were acquired at different field positions of the Gd(III) spectrum (see Figure 12 of the main text) at 10 K and a mixing time of 24 μs . From left to right: Primary RIDME data (solid line) and corresponding background fit (red dashes line), background corrected form factor (solid line) and its fit (red dashed line), resulting distance distribution. The color coding of the solid lines corresponds to a set of overtone coefficients and is retained throughout the figure. The pulse length, identical for $(\pi/2)$ and (π) pulses, is given in the figure next to the corresponding distance distributions.

Calibration of overtone coefficients for a series of Gd-rulers

Table S1 summarizes the data sets on which the calibration was performed. For calibration a wider range of overtone coefficients was scanned for a measurement of the Gd-ruler **13**. From that initial scanning procedure, a smaller set of coefficients $\{P_2 = 0.46, 0.40, 0.35\} \otimes \{P_3 = 0.05, 0.09\}$ was selected and applied to all data sets of Table S1. Note that in some cases other variations were tested as well, but did not result in further improvement of distance distribution as well as form factor fit in time and frequency domain at the same time. It is important to keep in mind that a good fit does not necessarily imply a clean distance distribution (Figure S16a). Likewise, a poor fit does not necessarily imply a wrong distance distribution (Figure S16b). Thus, the major criteria for calibration was to find the best compromise between form factor/ dipolar spectrum fit and clean anticipated distance distribution.

Over all data sets it was found that the set $\{P_1 = 0.51; P_2 = 0.40; P_3 = 0.09\}$ gives the best compromise between anticipated distance distribution and form factor/dipolar spectrum fit. As can be seen from Figures S17-S20, some slight variation of the optimal coefficients is observed with changing spin-spin distance (see Figure captions for values). For short spin-spin distance the chosen combination rather over-corrects the harmonic contribution (artefact peaks on right side of mean distance), while for long distance the chosen combination rather under-corrects (artefact peaks on left side of mean distance) the measured data. Nevertheless, for all measurements, the anticipated distance distribution and reasonable form factor/dipolar spectrum fits are obtained with the chosen coefficients (see Figures S17-S20 for the artefact levels). The remaining artefact level is smaller than typical distortions in distance distributions for biological samples that stem from noise or from small amounts of unfolded or aggregated material. Further, these coefficients were applied to all other measurements (Figures S21-S22 and Table S2), giving relatively clean distance distributions and form factor/ dipolar spectrum fits. For some cases the detected RIDME time trace is rather short compared to the distance of interest. This induces an uncertainty in the background correction and might be the reason for an overall higher artefact level in the resulting distance distribution. On top, due to incomplete phase cycling, many measurements exhibit the bump-like artefact at about zero time inducing distance peaks < 3 nm. Such artefacts do not change with the choice of overtone coefficients. Still, as described in the main text, other effects might be responsible for the remaining artefacts. A validation tool incorporated into *OvertoneAnalysis* can help to identify overtone-specific artefacts from other artefacts (see Figure 8 of the main part). In any case, validation is required if smaller side peaks are to be interpreted.

Moreover, the whole data set (Figures S18-S23) suggests, that RIDME form factors are stable with mixing time and approximately stable with temperature. With respect to these properties only small variations in the order of 0.05 for the ‘best coefficients’ are observed and we think it is reasonable to use one common set of coefficients for analysis. Moving the detection position away from the field maximum (Figure S21 d,e and Figure 13) does have a larger, systematic influence towards an under-correction of overtone coefficients (artefact peaks on left side of mean distance). The suggested under-correction is further supported by the deviation of experimental and fitted form factor.

Figure	Gd-ruler	Expected distance/ nm	Temperature/ K	Mixing time/ μs
Figure S17	2₁	3	10	24, 48, 72
			20	24
Figure S18	1₃	3.4	10	4, 8, 16, 24, 48
			20	4, 8, 16, 24
			30	4, 8, 16
Figure S19	2₂	4.3	10	4, 8, 16, 24, 48
			20	4, 8, 16, 24
			30	4, 8, 16
Figure S20	1₇	6.0	10, 25uM	16, 24
			20, 25 uM	24

Table S1: Summary of measurements for which the overtone variation was performed and corresponding Figure number.

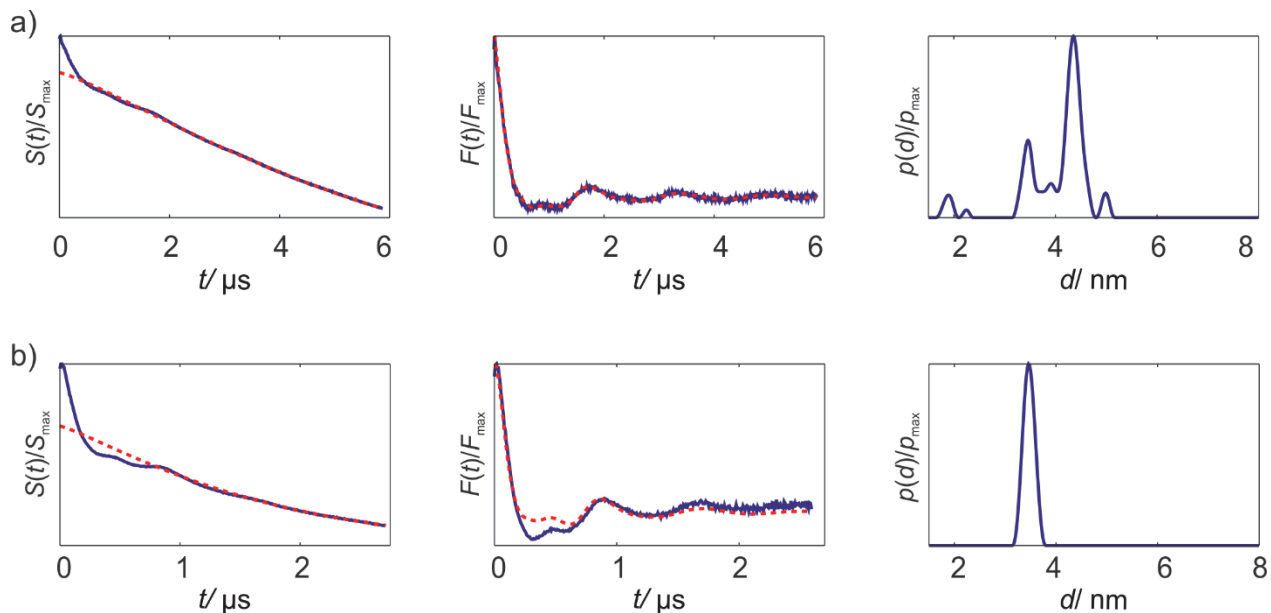


Figure S16: Pitfalls during regularization procedure with harmonic overtones. a) Good fit does not necessarily imply clean distance distribution. Gd-ruler **2₂** W band, 10 K 16 μs , $\{P_1 = 0.6; P_2 = 0.2; P_3 = 0.3\}$; b) Poor fit does not necessarily imply wrong distance distribution. Gd-ruler **1₃** W band, 20 K 16 μs , $\{P_1 = 0.4; P_2 = 0.4; P_3 = 0.2\}$.

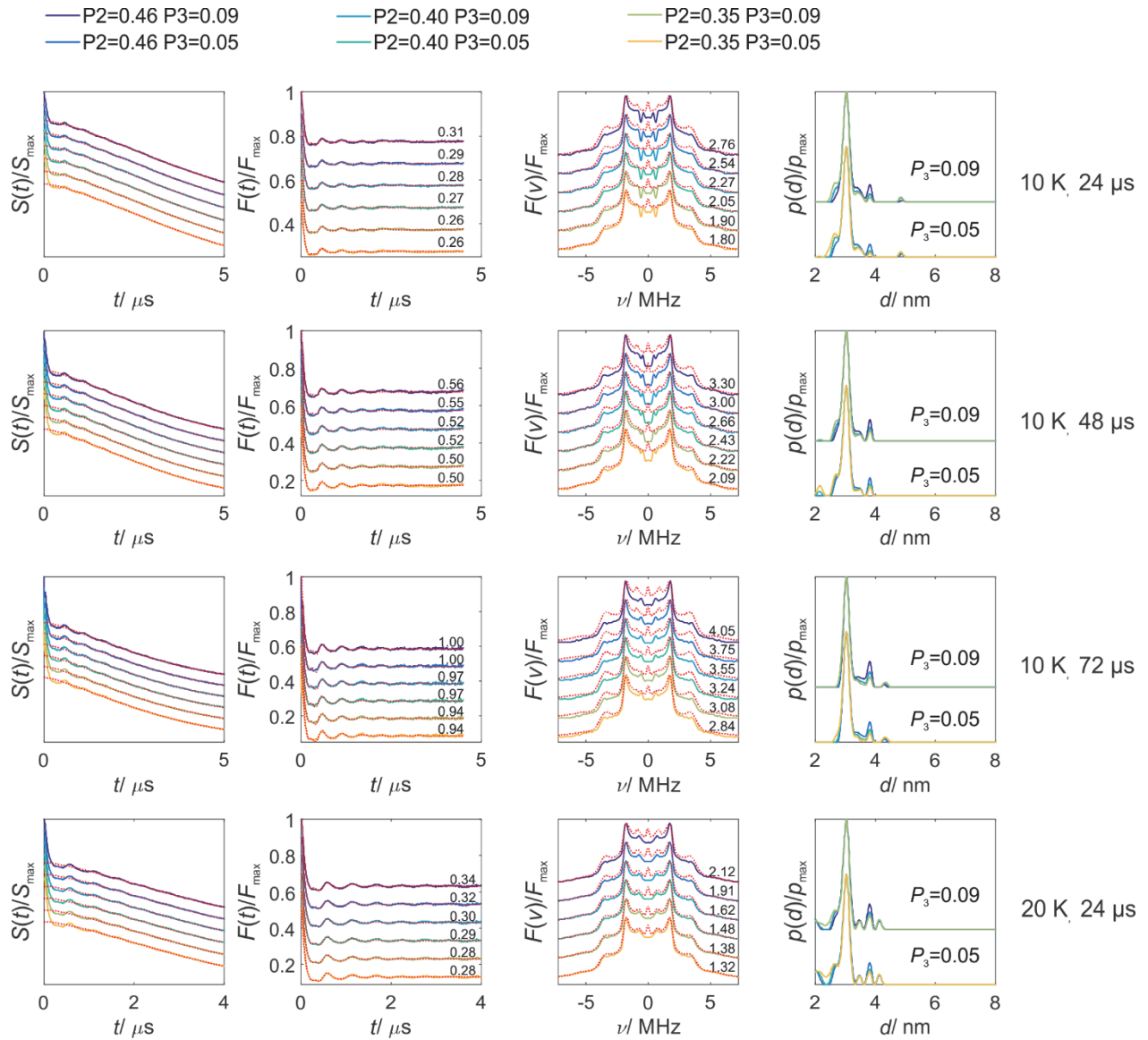
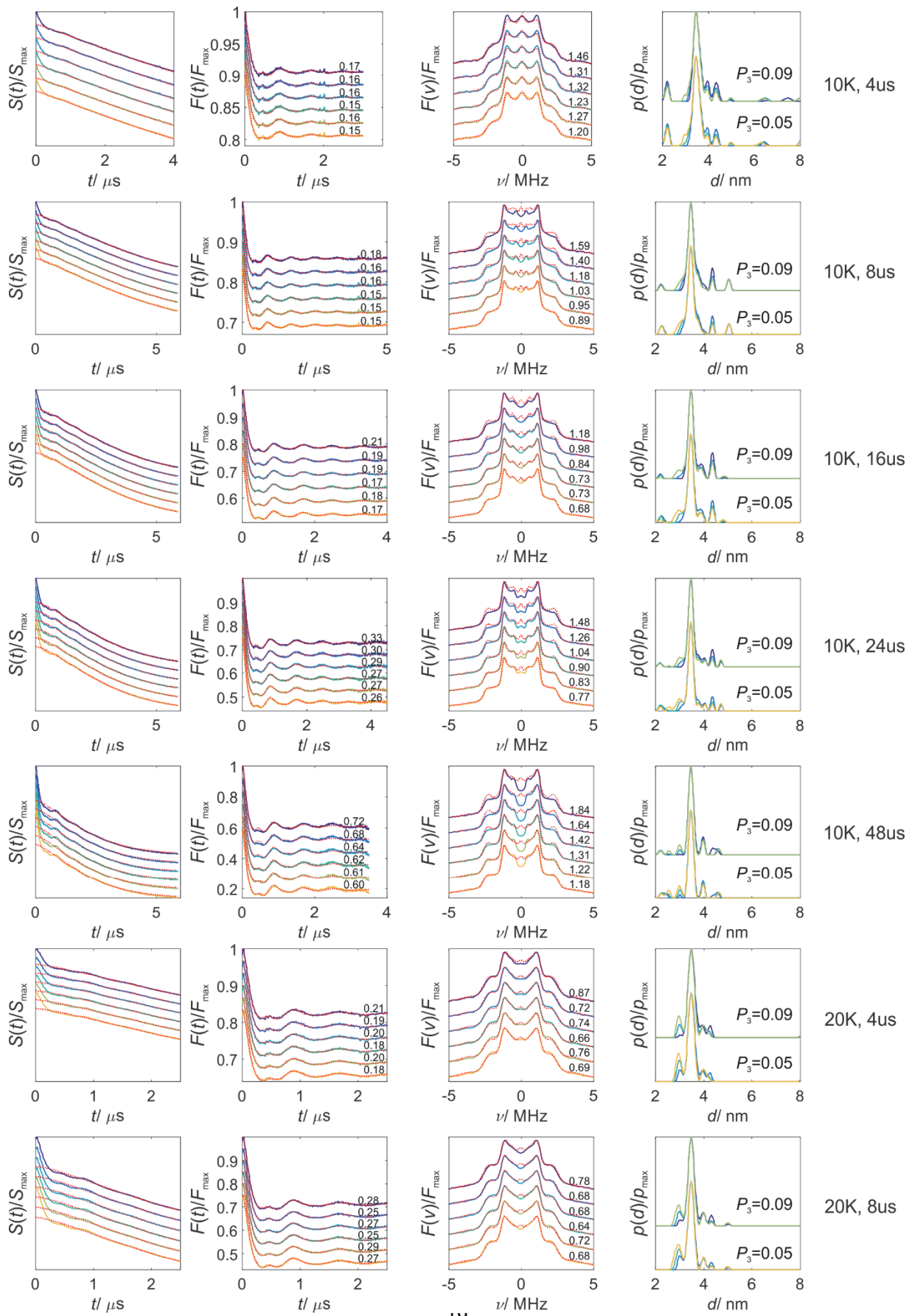


Figure S17: Calibration for Gd-ruler $\mathbf{2}_1$ at W band. Rows: Variation through overtone coefficients for a given measurement (temperature and mixing time). From left to right: Primary data, form factor in time domain, form factor in frequency domain and distance distribution. Upper lines in distance distribution $P_3 = 0.09$. Lower lines in distance distribution $P_3 = 0.05$. Top to bottom: increasing mixing time and temperature – exact numbers are given next to each row. RMSD values (multiplied by a factor of 100) between the data trace and the different fits are given next to the corresponding trace. It can be observed that artefact peaks shift from left to right or increase in intensity on the right side with respect to the mean distance for an increasing fraction of higher harmonics. On average the best compromise between distance distribution and form factor fit is obtained for $\{P_1 = 0.56; P_2 = 0.35; P_3 = 0.09\}$ or $\{P_1 = 0.55; P_2 = 0.40; P_3 = 0.05\}$, which indicates the uncertainty of the coefficients. Nevertheless, distance analysis using $\{P_1 = 0.51; P_2 = 0.40; P_3 = 0.09\}$ gives reasonable results in all cases.



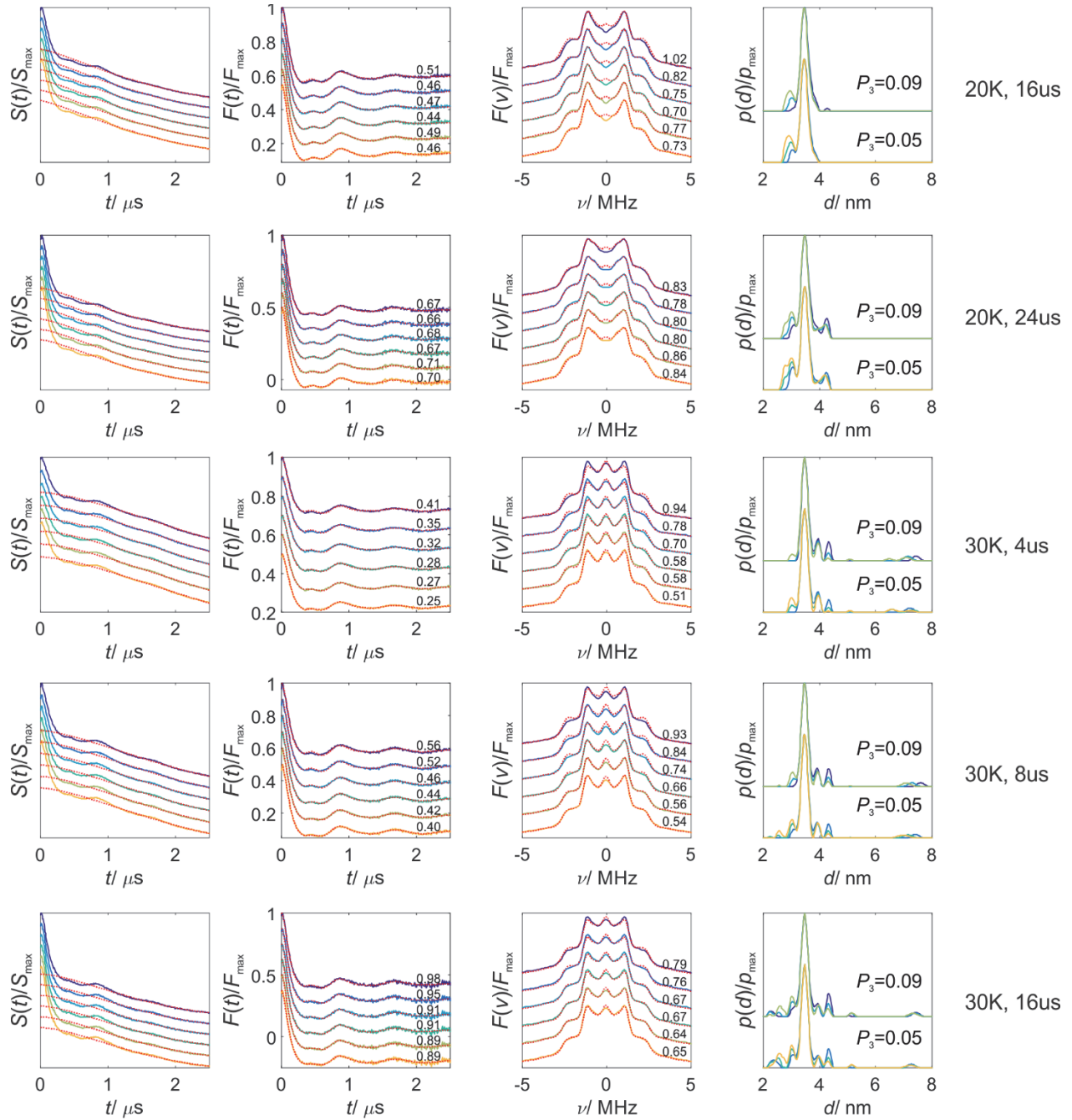
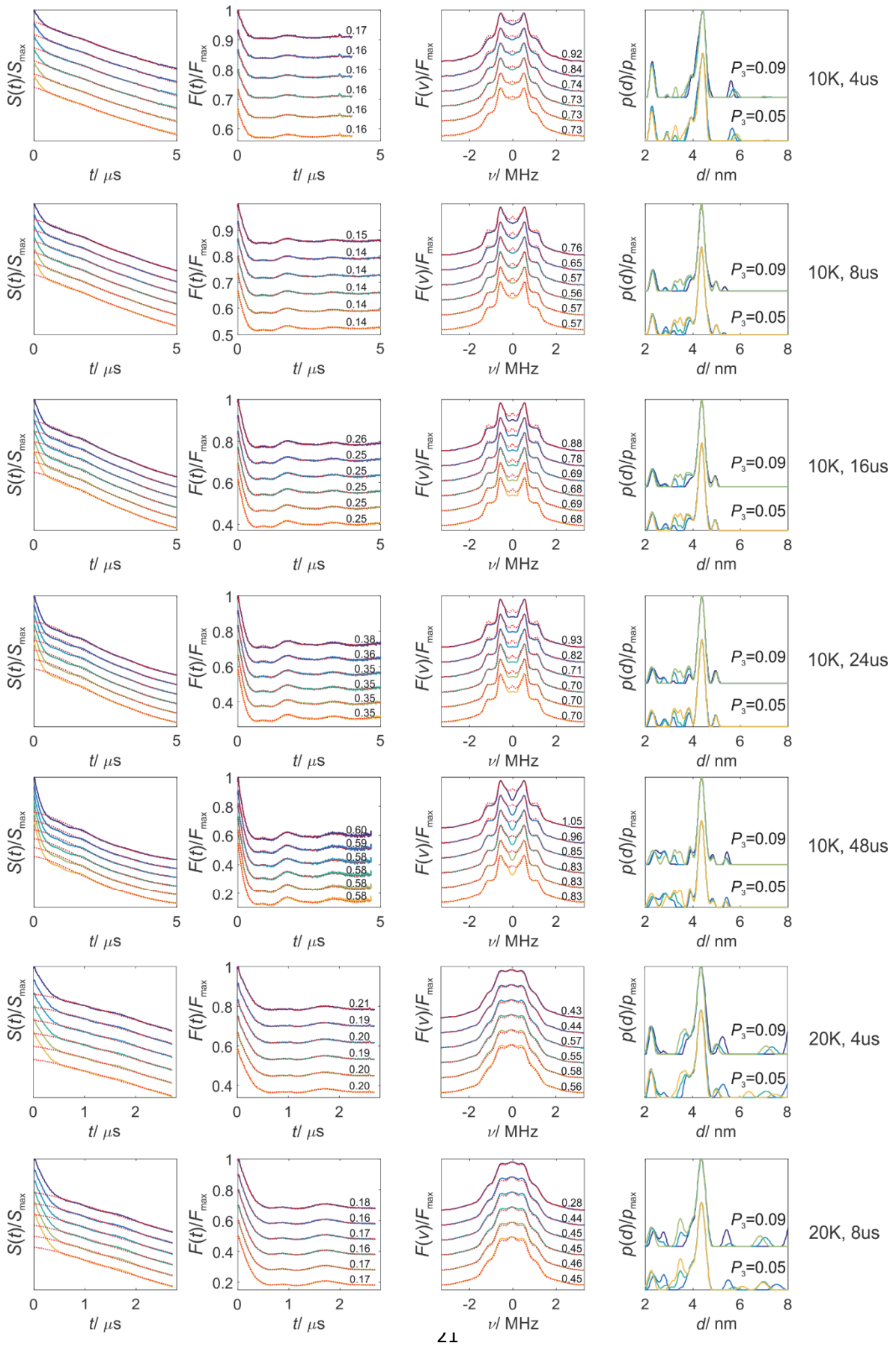


Figure S18: Calibration for Gd-ruler I_3 at W band. Rows: Variation through overtone coefficients for a given measurement. Color coding is maintained from Figure S17. From left to right: Primary data, form factor in time domain, form factor in frequency domain and distance distribution. Upper lines in distance distribution $P_3 = 0.09$. Lower lines in distance distribution $P_3 = 0.05$. Top to bottom: increasing mixing time and temperature – exact numbers are given next to each row. RMSD values (multiplied by a factor of 100) between the data trace and the different fits are given next to the corresponding trace. It is observed that artefact peaks do shift from left to right with respect to the mean distance for increasing higher harmonics. On average the best compromise between distance distribution and form factor fit is obtained for $\{P_1 = 0.51; P_2 = 0.40; P_3 = 0.09\}$ or $\{P_1 = 0.55; P_2 = 0.40; P_3 = 0.05\}$. The spikes observed in the two upper rows at 2 or 4 μs are most likely artefacts remaining from crossing echoes due to the incomplete decay of the transverse magnetization during the mixing block as the mixing time (4 or 8 μs) is relatively short compared to the phase memory time ($\sim 10 \mu\text{s}$).



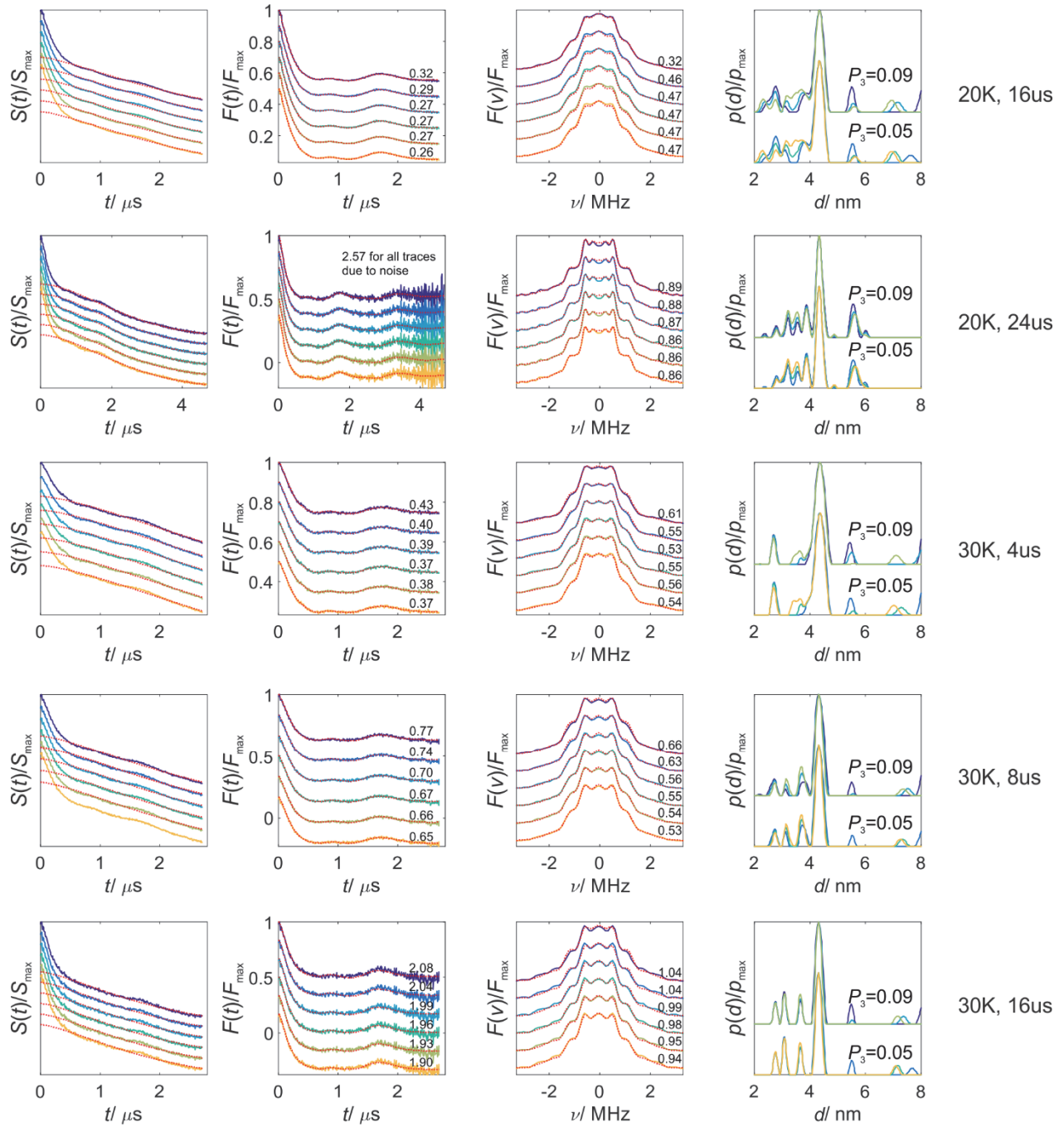


Figure S19: Calibration for Gd-ruler 2_2 at W band. Rows: Variation through overtone coefficients for a given measurement. Color coding is maintained from Figure S17. From left to right: Primary data, form factor in time domain, form factor in frequency domain and distance distribution. Upper lines in distance distribution $P_3 = 0.09$. Lower lines in distance distribution $P_3 = 0.05$. Top to bottom: increasing mixing time and temperature – exact numbers are given next to each row. RMSD values (multiplied by a factor of 100) between the data trace and the different fits are given next to the corresponding trace. On average, it can be observed that artefact peaks do shift from left to right with respect to the mean distance for an increasing fraction of higher harmonics. The best compromise between distance distribution and form factor fit is obtained for $\{P_1 = 0.51; P_2 = 0.40; P_3 = 0.09\}$.

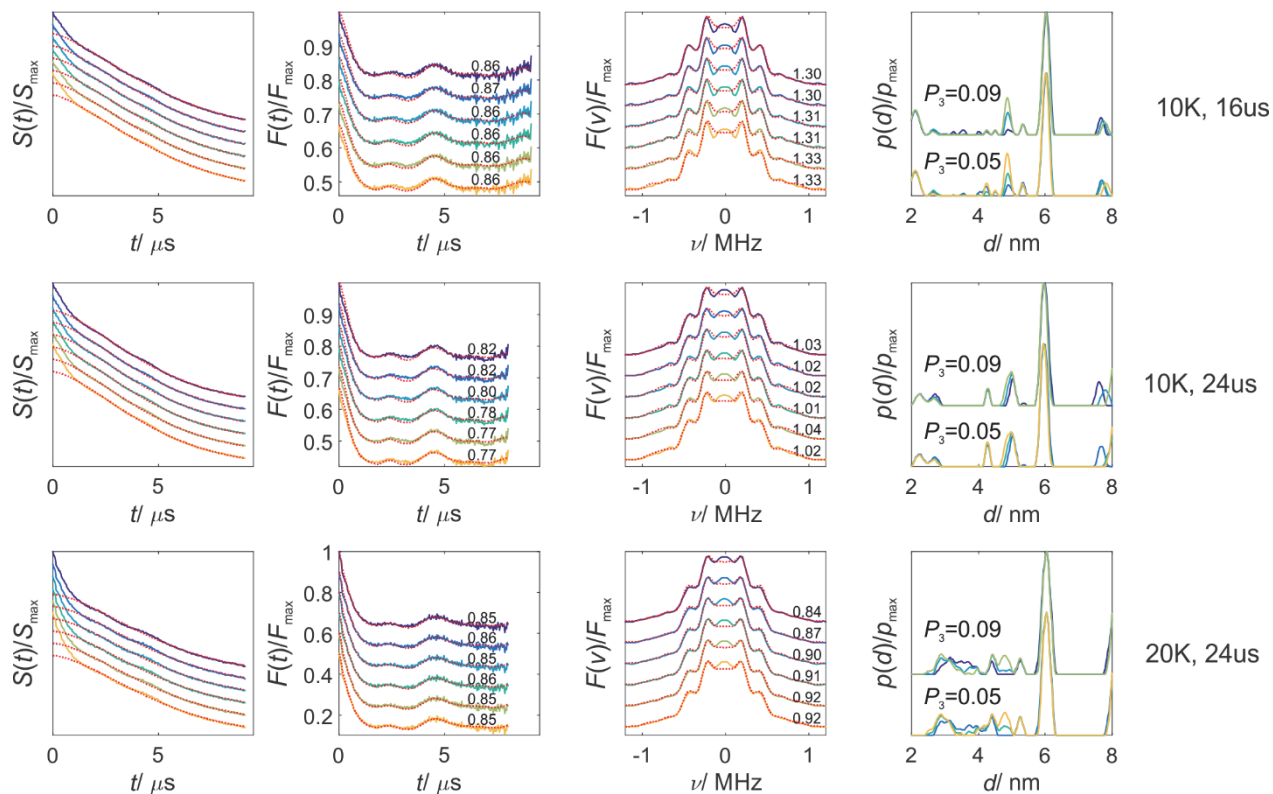


Figure S20: Calibration for Gd-ruler **17** at W band. Rows: Variation through overtone coefficients for a given measurement. Color coding is maintained from Figure S17. From left to right: Primary data, form factor in time domain, form factor in frequency domain and distance distribution. Upper lines in distance distribution $P_3 = 0.09$. Lower lines in distance distribution $P_3 = 0.05$. Top to bottom: increasing mixing time and temperature – exact numbers are given next to each row. RMSD values (multiplied by a factor of 100) between the data trace and the different fits are given next to the corresponding trace. In the cases presented here, it can be observed that artefact peaks do not shift from left to right with respect to the mean distance, but only decrease in intensity for increasing higher harmonics. The best compromise between distance distribution and form factor fit is obtained for $\{P_1 = 0.45; P_2 = 0.46; P_3 = 0.09\}$ or $\{P_1 = 0.49; P_2 = 0.46; P_3 = 0.05\}$. Nevertheless, distance analysis using $\{P_1 = 0.51; P_2 = 0.40; P_3 = 0.09\}$ gives reasonable results in all cases.

Figure	Gd-raker	Expected distance/ nm	Temperature/ K	Mixing time/ μ s
Figure S21	1₅	4.7	10	8, 12, 16, 24, 56, 120, 200 Field depend 24: max, -80G, -1500G
			20	8, 16, 24, 32, 40, 48, 56 Field depend 24: max, -80G, -1500G
			30	4, 24
Figure S22	mixture of 1₃ and 1₅	3.4 : 4.7	10	12, 24, 36
			20	12, 24
			30	12

Table S2: Summary of measurements for which the set of overtone coefficients $\{P_1 = 0.51; P_2 = 0.40; P_3 = 0.09\}$ was applied.

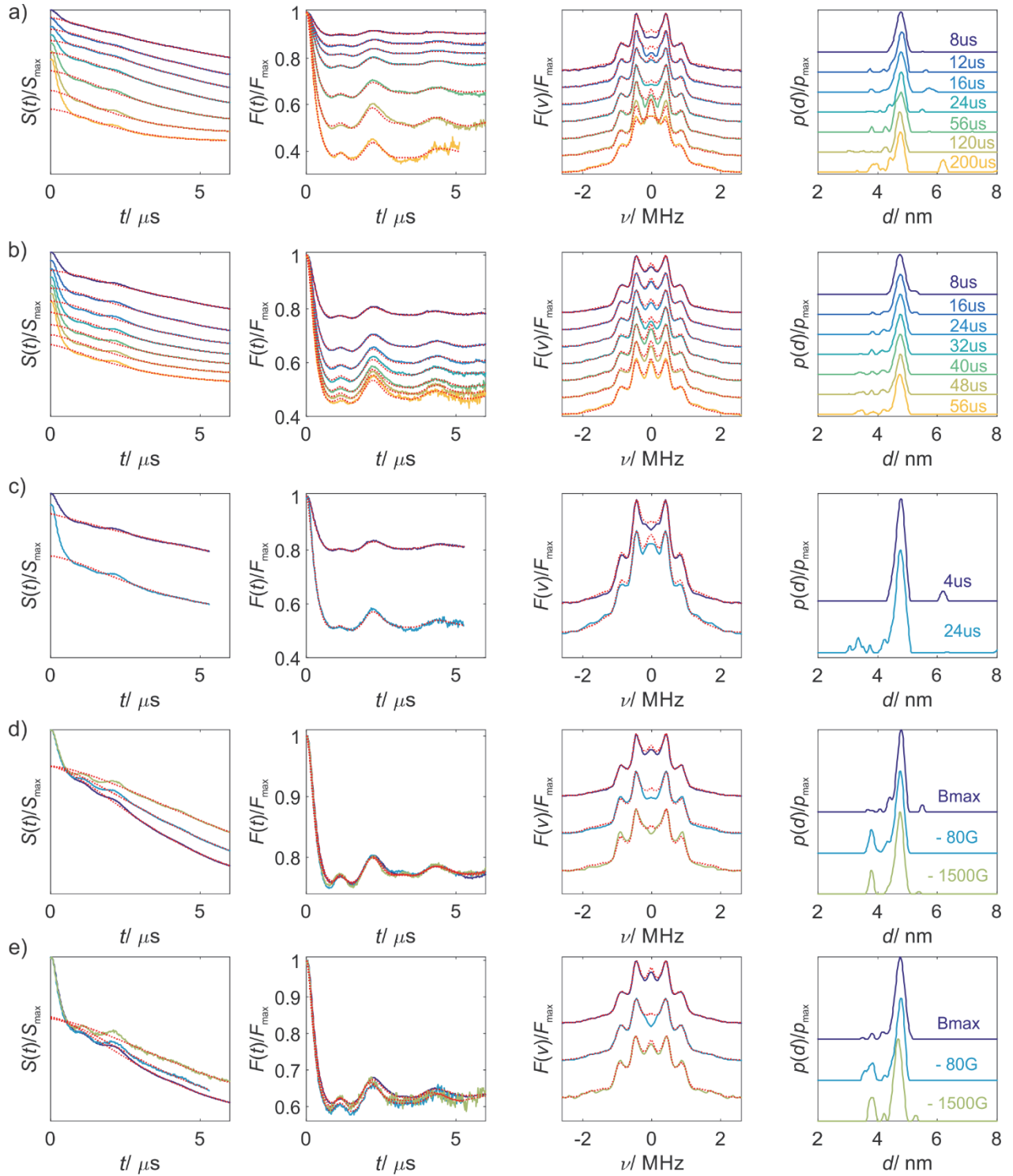


Figure S21: Data for Gd-ruler 1_5 at W band. Raw data was truncated for the bump artefact at zero time. From left to right: Primary data, form factor in time domain, form factor in frequency domain and distance distributions using coefficients $\{P_1 = 0.51; P_2 = 0.40; P_3 = 0.09\}$. Form factors and distance distributions remain rather stable for different temperatures and mixing times. a) 10 K, b) 20 K, c) 30 K, d) field dependence at 10 K (24 μs mixing time) and e) field dependence at 20 K (24 μs mixing time).

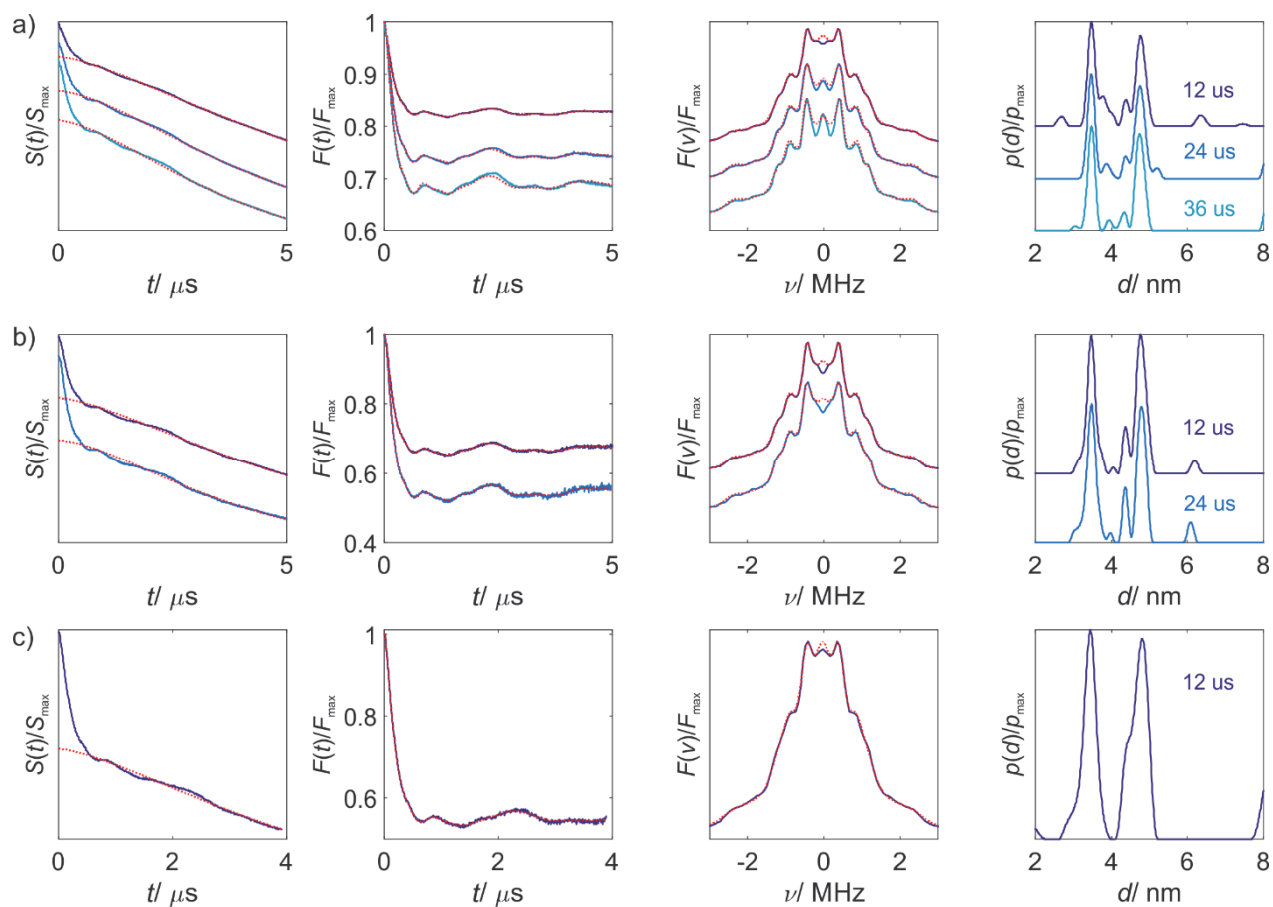


Figure S22: Data for the mixture of Gd-rulers **13** and **15** at W band. From left to right: Primary data, form factor in time domain, form factor in frequency domain and distance distribution using the set of coefficients $\{P_1 = 0.51; P_2 = 0.40; P_3 = 0.09\}$. Form factors and distance distribution remain rather stable for different temperatures and mixing times. a) 10 K, b) 20 K and c) 30 K.

References:

- 1 G. Jeschke, V. Chechik, P. Ionita, A. Godt, H. Zimmermann, J. Banham, C. R. Timmel, D. Hilger and H. Jung, *Appl. Magn. Reson.*, **30**, 473–498, <http://www.epr.ethz.ch/software.html>.
- 2 S. Razzaghi, M. Qi, A. I. Nalepa, A. Godt, G. Jeschke, A. Savitsky and M. Yulikov, *J. Phys. Chem. Lett.*, 2014, **5**, 3970–3975.
- 3 A. Doll, M. Qi, A. Godt and G. Jeschke, *J. Magn. Reson.*, 2016, **273**, 73–82.